

Nanometer-localized multiple single-molecule fluorescence microscopy

Xiaohui Qu^{*†}, David Wu^{*‡§}, Laurens Mets[¶], and Norbert F. Scherer^{*‡||}

Departments of ^{*}Physics, [¶]Molecular Genetics and Cell Biology, and [‡]Chemistry and [†]Institute for Biophysical Dynamics, University of Chicago, Chicago, IL 60637

Edited by Robert Haselkorn, University of Chicago, Chicago, IL, and approved June 23, 2004 (received for review March 26, 2004)

Fitting the image of a single molecule to the point spread function of an optical system greatly improves the precision with which single molecules can be located. Centroid localization with nanometer precision has been achieved when a sufficient number of photons are collected. However, if multiple single molecules reside within a diffraction-limited spot, this localization approach does not work. This paper demonstrates nanometer-localized multiple single-molecule (NALMS) fluorescence microscopy by using both centroid localization and photobleaching of the single fluorophores. Short duplex DNA strands are used as nanoscale “rulers” to validate the NALMS microscopy approach. Nanometer accuracy is demonstrated for two to five single molecules within a diffraction-limited area. NALMS microscopy will greatly facilitate single-molecule study of biological systems because it covers the gap between fluorescence resonance energy transfer-based (<10 nm) and diffraction-limited microscopy (>100 nm) measurements of the distance between two fluorophores. Application of NALMS microscopy to DNA mapping with <10-nm (i.e., 30-base) resolution is demonstrated.

It is well known that the spatial resolution of an optical system is limited by the Rayleigh criterion (1),

$$d_R = 0.61\lambda/N.A., \quad [1]$$

where λ is the wavelength of the collected photons and N.A. is the numerical aperture of the system. Using visible light (i.e., ≈ 500 nm) and a high N.A. objective (i.e. >1) allows achieving ≈ 250 -nm lateral resolution. However, most biological macromolecules (DNA, RNA, proteins, etc.) and molecular machines (e.g., ribosome and spliceosome) are much smaller in two or all three dimensions, with important features or subassemblies lying within 10 nm of each other (2).

Fluorescence resonance energy transfer (FRET) is widely used for studying biological systems on the nanometer scale (i.e., <10 nm; ref. 3). FRET occurs over distances similar to the Förster radius, which is ≈ 5 nm for common fluorophores (4). However, FRET only gives the relative distance between two probes, whereas their absolute positions remain unknown. Centroid localization, which has been used for single-particle tracking, allows determination of the centroid position of the particle to a much better precision than the length scale defined by the Rayleigh criterion (5–7). Recently, this approach to localizing fluorophores has been applied to single dye molecules (Cy3 and Rhodamine dyes) bound to molecular motors, and 2-nm precision in localization has been achieved when an oxygen scavenging buffer was used to suppress photobleaching (8, 9). However, centroid localization can only be used for isolated single molecules and it does not improve the resolution of the imaging system. It has been shown that two probes with different fluorescent wavelengths can be resolved within 10 nm because they are spectrally distinguishable (10). This method does not help when two or more objects with the same emission spectrum are within a diffraction-limited spot. Imaging applications beyond even the capabilities of “superresolution” microscopy (11) and without the complexity inherent to near-field scanning optical microscopy (12), such as the distribution and disposition

of components of molecular complexes and “machines” (2) and their motions, would benefit from approaches with few nanometer resolution.

Whereas DNA sequencing provides detailed information that is essential for understanding the function and evolution of genes and their flanking regions, whole-genome characterization provides the genetic context in which these functions and changes take place (13–15). Although much progress has been made in the assembly of large-genome regions from raw sequence data, the short scope of individual sequencing reactions (on the order of 1 kb) makes complete genome characterization by sequencing alone an extremely challenging task (16, 17). Optical mapping of much longer (100–1,000 kb) single DNA molecules, by using gaps generated by digestion with restriction endonucleases as landmark sites, has provided a breakthrough method of comparatively rapid whole-genome characterization with the potential to complement and support whole-genome sequencing efforts (18). Whereas optical mapping provides a valuable approach for comparative genomics, the information content of these maps is restricted by dependence on an imaging method whose resolution is limited by the Rayleigh criterion. Given an imaging method with much better resolution, optical mapping of DNA molecules by using fluorescent tags bound to specific sequence-recognition sites could be exploited to dramatically increase the information content of long-range physical mapping and of whole-genome characterization.

This paper demonstrates nanometer-localized multiple single-molecule (NALMS) fluorescence microscopy, a method that makes use of centroid localization and exploits the inevitable photobleaching of single fluorophores to achieve nanometer-scale resolution of single-molecule fluorophores. The resolution obtainable with this approach is demonstrated for two identical fluorophores (i.e., Cy3) separated by 8 nm with 2.5-nm precision for the distance determination and depends on the total number of photons collected for each fluorophore. The method can be easily extended to multicolor applications. This paper also demonstrates that NALMS fluorescence microscopy is an attractive approach for ultraresolution DNA mapping. Single fluorophores are attached to specific 7-base sequences on DNA by peptide nucleic acid (PNA) labeling and NALMS fluorescence microscopy is used to determine the fluorophore locations with <10 -nm (i.e., 30-base) resolution.

Materials and Methods

Sample Preparation for DNA Ruler Test. Because duplex DNA has a 50-nm persistence length (19), it can be considered to be a rigid

This paper was submitted directly (Track II) to the PNAS office.

Abbreviations: NALMS, nanometer-localized multiple single-molecule; FRET, fluorescence resonance energy transfer; PNA, peptide nucleic acid; TIRF, total internal reflection fluorescence; CCD, charge-coupled device.

[§]Present address: David Geffen School of Medicine, University of California, Los Angeles, CA 90095.

^{||}To whom correspondence should be addressed at: 5735 South Ellis Avenue, SCL 033, Chicago, IL 60637. E-mail: nfschere@uchicago.edu.

© 2004 by The National Academy of Sciences of the USA

rod “ruler” on the 10- to 20-nm length scale. The DNA rulers used were 40-base duplex DNA (sequence 5'-Cy3-GAA CCA GTT TCC ATA AAG GAC CCA GAA TCC GAT AGG ACC G-biotin-3') and 24-base DNA (sequence 5'-Cy3-AGG ACC CAG AAT CCG ATA GGA CCG-biotin-3'). Both were hybridized with the complementary strands, also labeled with Cy3 at the 5' end and biotin at the 3' end, and were purified by gel electrophoresis to eliminate single strands that had not hybridized. The DNA rulers were stored at 4°C in TE buffer (10 mM Tris/1 mM Na₂EDTA, pH 8.0) and the experiment was performed at room temperature (17°C). The DNA duplexes were stable for at least several months under the experimental condition.

DNA labeling and surface immobilization was performed with some modification of published procedures (20, 21). No. 1 coverslips were soaked in 2% hydrofluoric acid solution for 10 min, rinsed with water, and dried with nitrogen gas. A small chamber was made with two coverslips and 3M double-sided tape. Fifty microliters of 1 mg/ml BSA-biotin (Sigma, catalog no. A-8549) in TE buffer was added to the chamber, allowed to sit for 10 min, and was then washed with 100 μl of TE buffer. Fifty microliters of 0.2 mg/ml streptavidin (Molecular Probes, catalog no. S-888) in TE buffer was then added, allowed to sit for 10 min, and the protein-coated coverslip was washed with 100 μl of TE buffer. A 3 nM solution of Cy3- and biotin-labeled 24-base or 40-base duplex DNA solution in TE buffer was mixed with 10 mg/ml BSA (Behring Diagnostics, catalog no. 126575) by 1:9 (vol/vol). Fifty microliters of the mixture was added to the chamber, allowed to sit for 10 min, and was then washed with 200 μl of TE buffer. One hundred microliters of imaging buffer was added and the chamber was sealed with nail polish. The imaging buffer contains TE buffer with 30 mg/ml glucose, 0.1 mg/ml glucose oxidase (Sigma-Aldrich, catalog no. G-7016), 0.2 mg/ml catalase (Roche Diagnostics, catalog no. 106810), 1% (vol/vol) 2-mercaptoethanol, and 10 mM MgCl₂. These enzymes remove molecular oxygen in solution, thereby reducing the rate of irreversible photobleaching of the dye molecules (8).

Sample Preparation for DNA Mapping. Coverslips were cleaned as described for the DNA ruler measurement. Fifty microliters of 0.015% 3-aminopropyltrimethoxysilane (Aldrich, catalog no. 28177-8) in acetone was sandwiched between two coverslips and incubated for 15 min. The coverslips were separated, rinsed with acetone, then with water, and were then dried with nitrogen gas. A drop of Alexa 488-bis-PNA-labeled λ-DNA solution was placed on one functionalized coverslip. The DNA was spread by dynamic molecular combing by rolling the drop across the coverslip (22). Fifty microliters of 20% 2-mercaptoethanol was added and covered with another coverslip. This sandwich was sealed with nail polish.

Binding fluorophore-labeled bis-PNA to DNA is accomplished by incubating the mixture of 12 μM Alexa 488-bis-PNA (sequence: Alexa 488-eg1-TTTCTCC-eg1eg1eg1-CCTCTTT-amide; ref. 23) and 12.5 nM λ-DNA (New England Biolabs, catalog no. N3013L) in 100 mM phosphate buffer (30 mM Na₂HPO₄/70 mM NaH₂PO₄, pH 6.6) at a decreasing temperature, beginning at 80°C and decreasing 1°C every 5 min to 4°C. The DNA/PNA complexes were separated from free PNA by ethanol precipitation and were then resuspended in water.

Total Internal Reflection Fluorescence (TIRF) Microscope. All single-molecule- and dual-fluorophore-labeled DNA ruler test data were obtained by using a home-built objective-type TIRF microscope, based on an Olympus (Melville, NY) IX71 inverted fluorescence microscope and a ×60 objective (Olympus, N.A. = 1.45, oil immersion). A 532-nm laser [New Focus (San Jose, CA), model no. 3951-20, 20 mW power] was used as the illumination source. An OD = 1 neutral density filter was used for most

experimental results shown. The incident laser power at the TIR interface is roughly 0.5 mW, illuminating a circular region 40 μm in diameter. Due to the Gaussian profile of the laser beam, the illumination intensity is higher in the center of the area than at the periphery. Thus, the emission intensity (number of photons collected per unit time) depends on the location of dye molecules. Furthermore, even within a diffraction-limited spot, the fluorescence emission intensity of individual dye molecules may exhibit variability, presumably resulting from differences in the local environment and the way the dyes bind to the DNA and orientations created by the BSA/streptavidin/biotin double tether. The emitted photons were collected through a filter cube [Chroma (Rockingham, VT) Q560LPBS, HQ585/40M], magnified by a ×3.3 eyepiece (Olympus) and detected by a back-illuminated, TE-cooled, frame-transfer charge-coupled device (CCD) detector [Andor, DV435-BV (South Windsor, CT)] with 1,024 × 1,024 13-μm square pixels. The effective pixel size of the CCD detector due to magnification of the ×60 objective and the ×3.3 eyepiece is 65.7 nm (which is parameter *a* in Eq. 3). The width of the point spread function of the setup (*S_x* and *S_y* in Eq. 2) is *S_{xy}* = 1.9 pixels, which is 124.8 nm. One count from the CCD detector corresponds to roughly two collected photons (Andor system performance booklet). For most of the data shown, the CCD was operated in frame transfer mode, cooled to -50°C, with 1 s of integration time for each frame and <1 ms of dead time between frames (i.e., the frame transfer time).

Centroid Localization. It has been shown that the centroid of a diffraction-limited image of a point object can be localized to high precision by fitting the collected distribution of photons/counts (i.e., the image) to the point spread function of the system (24). This is usually well approximated by a two-dimensional Gaussian fit,

$$N_{xy} = B + N_{00} \times \exp\left[-\frac{(x - x_0)^2}{2S_x^2} - \frac{(y - y_0)^2}{2S_y^2}\right], \quad [2]$$

where (*x*₀, *y*₀) is the centroid of the point source, *N_{xy}* and *N*₀₀ are the counts (or photons collected) at pixel (*x*, *y*), and at the centroid position (*x*₀, *y*₀) on the CCD detector, *S_x* and *S_y* are the width of the point spread function in the *x* and *y* directions, and *B* is the baseline. The baseline includes the CCD detector background, readout noise, and residual scattered light. The SE in centroid localization is well estimated by

$$\sigma_{i0}^2 = \frac{S_i^2 + a^2/12}{N} + \frac{8\pi S_i^4 b^2}{a^2 N^2}, \quad [3]$$

where *i* = *x* or *y*, *N* is the total counts for the image, *a* is the effective pixel size of the detector, and *b* is the SD of background noise.

Later in this paper, we will study the distance between two fluorophores. Because distance is calculated from the centroid location of two fluorophores as

$$d = [(\Delta x_0)^2 + (\Delta y_0)^2]^{1/2} = [(x_{01} - x_{02})^2 + (y_{01} - y_{02})^2]^{1/2},$$

the SE in the distance measurement can be calculated from the uncertainty of the centroid localization of each of the two fluorophores (Eq. 3) as in ref. 8:

$$\begin{aligned} \langle (\Delta d)^2 \rangle &= \frac{(\Delta x_0)^2}{(\Delta x_0)^2 + (\Delta y_0)^2} \times (\sigma_{x01}^2 + \sigma_{x02}^2) \\ &+ \frac{(\Delta y_0)^2}{(\Delta x_0)^2 + (\Delta y_0)^2} \times (\sigma_{y01}^2 + \sigma_{y02}^2). \end{aligned} \quad [4]$$

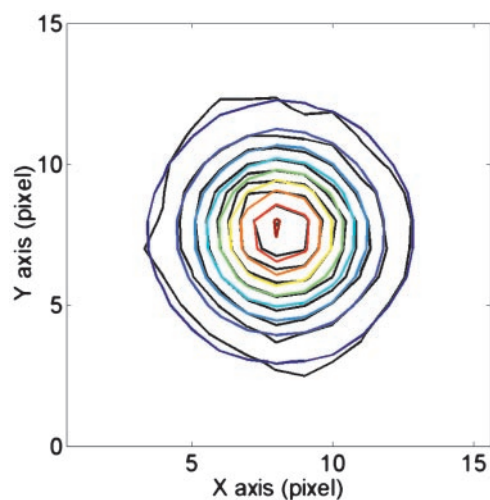


Fig. 1. Contour plots of the CCD image of a Cy3 dye molecule (black) and a two-dimensional Gaussian function (Eq. 2; color), which is used as a point-spread function to fit the image. The fit gives $x_0 = 7.57$ (pixel), $y_0 = 8.17$ (pixel), $S_x = S_y = 1.9$ pixels, $N_{00} = 442$ counts, and $b = 10$ counts, and 10,143 total counts are collected. Eq. 3 gives $\sigma_{x0} = \sigma_{y0} = 1.7$ nm.

The 1-s integration time used in the present experiment is much longer than the period of the thermal motion of the fluorophores, DNA and BSA/streptavidin/biotin tether. Assuming the thermal motion is symmetric about the tether point, it will not affect the centroid determination of the dye position or the distance measurement between two dyes.

Photobleaching of Single Fluorophores. Single fluorophores have the signature of almost constant emission intensity when the collection time is much longer than the “blinking” period and terminating with abrupt photobleaching (25). Photobleaching is a Poisson process that obeys an exponential distribution,

$$P(t) = \frac{1}{\tau} e^{-t/\tau},$$

where $P(t)$ is the probability that the fluorophore photobleaches at time t , while τ is the time constant for photobleaching. Note that τ depends on many molecular photophysical parameters (absorption cross section, intersystem crossing time, etc.) and external variables (e.g., focused laser intensity, concentration of singlet oxygen, etc.). Thus, for a collection of a few fluorophores within a diffraction-limited spot, sudden step changes in fluorescence intensity will be observed with the number of steps equal to the number of fluorophores.

Results and Discussion

Centroid Localization and Photobleaching of Single Molecules. Fig. 1 shows a contour plot of the count distribution over the pixels of the CCD detector associated with imaging a single Cy3 fluorophore with the TIRF microscope. The contour for the Gaussian fit through Eq. 2 is superimposed on the data, allowing determination of the point spread function of the microscope. Fig. 2 shows the time course of fluorescence emission from a single fluorophore, displaying the counts recorded at the “peak count” pixel of the image. The 1-s integration time used in the experiment is much longer than the blinking period of Cy3 dyes. An almost constant emission intensity with small fluctuations is observed for the Cy3 dye emission. Sudden photobleaching is observed after 300 s of data collection; the counts drop to the background level, thereby proving the detection of only a single fluorophore. Fig. 2 *Inset* shows the histogram for the counts at

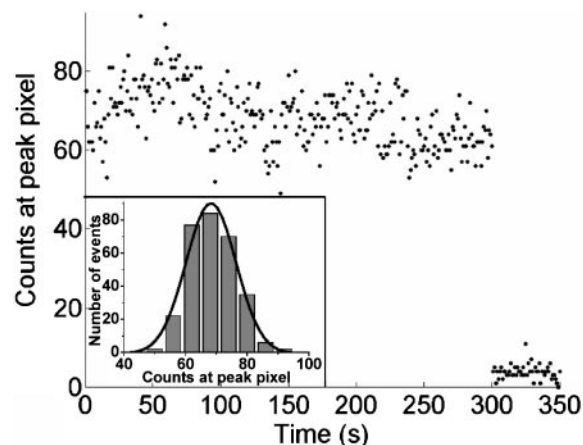


Fig. 2. Time trace of a single Cy3 dye molecule. The counts at the peak pixel of the CCD image are plotted against time. The dye exhibits sudden photobleaching at 300 s and the counts drop to a background level afterward. (*Inset*) Histogram of the collected counts at the peak pixel before photobleaching. The Gaussian fit gives the collected counts as 68 ± 8 , where 8 is the width of the Gaussian fit.

the peak pixel before photobleaching. A Gaussian fit yields 68 counts for the mean value and the SD, given by the width of the Gaussian fit, is 8 counts.

When multiple point sources are very close to each other, i.e., within the limit set by the Rayleigh criterion of Eq. 1, centroid localization would identify them as a single source and give the average position. However, by making use of the sudden photobleaching of single fluorophores, multiple dyes can be resolved. The appropriate parts of the time trace can be used to locate the centroid position of each fluorophore to nanometer precision, provided that enough photons are collected. Thus, nanometer resolution for multiple fluorophores is achieved by associating the appropriate count distributions with each fluorophore. Three fluorophores are resolved for the example shown in Fig. 3. Interval 1 of the trace where only fluorophore

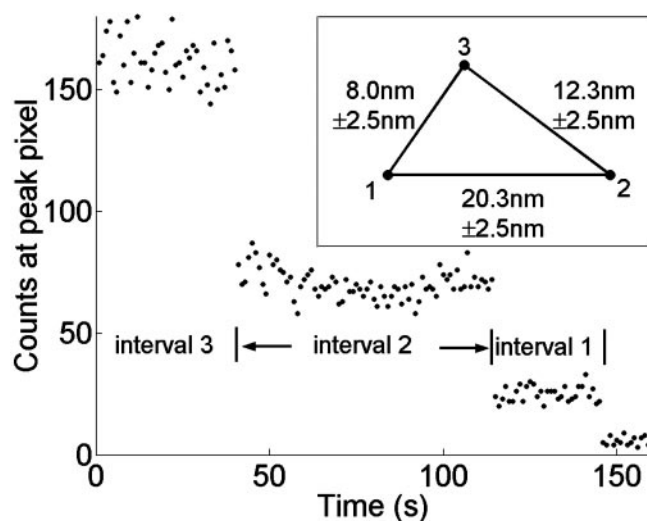


Fig. 3. Time trace of three Cy3 dyes within the point-spread function of the microscope. The number of counts collected at the peak pixel of the CCD image is essentially constant (with statistical fluctuations) over time with three sudden photobleaching events. The dyes are resolved and localized as described in the text. (*Inset*) The resultant distances between the fluorophores thus determined are $d(1, 2) = 20.3 \pm 2.5$ nm, $d(1, 3) = 8.0 \pm 2.5$ nm, and $d(2, 3) = 12.3 \pm 2.5$ nm.

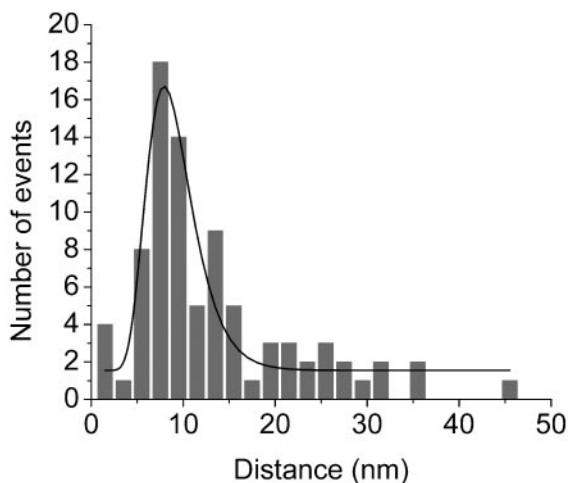


Fig. 4. Histogram of the end-to-end distance measurements of a 24-base DNA ruler. The lognormal fit gives the end-to-end distance as $[8 - 2, 8 + 3]$ nm where 8 nm is the location of the center of the lognormal fit, and 2 nm and 3 nm are the width of the fitted function for the region to the left and to the right of the center, respectively.

1 is still fluorescent can be used to localize the centroid of fluorophore 1. Because of the almost constant intensity of fluorophore 1 before photobleaching, the location and average counts per frame obtained in interval 1 are assumed to be a good approximation of its location and counts per frame in interval 2 of the trace. Subtracting the fluorescence distribution of fluorophore 1 from the distribution in interval 2 leaves the signal from fluorophore 2. This distribution is used to localize the centroid of fluorophore 2. Similarly, the signal left in interval 3 after subtracting the contributions of fluorophores 1 and 2 is used to localize the centroid of fluorophore 3. The relative locations of the three fluorophores are shown in Fig. 3 *Inset*. For events with even more fluorophores, this process can be continued until all of the fluorophores are localized; this has been achieved with up to five fluorophores (see Fig. 8, which is published as supporting information on the PNAS web site).

Sometimes an almost totally “off” state lasting from one to a few frames is observed before a dye molecule photobleaches. Also after a dye photobleaches, it might occasionally come back to the “on” state for a very short period. The data points of these discrete off and on states are excluded from the analysis (see Fig. 8). Some dyes showing “abnormal” changes in the emission intensity over time are also observed. These intensity changes are usually slow and smooth in comparison with the sudden photobleaching of dyes. In such cases, multiple dyes can still be resolved as long as sudden photobleaching events can be identified; the dyes can be localized by using only the frames shortly before and after the photobleaching event. However, to avoid any ambiguity in testing the NALMS microscopy method, dyes with abnormal intensity change are not included in the histograms in the DNA ruler verification experiment discussed in the next subsection.

Verification of Nanometer Localization with Nanoscale Rulers. To test the accuracy of NALMS microscopy, 24- and 40-base double helix DNA molecules labeled at both ends with Cy3 dyes and biotin are used as nanoscale rulers (see *Materials and Methods*). A series of images are taken until all of the fluorophores photobleach. NALMS position analysis is used to resolve the multiple dyes as described in the previous subsection and the distance between the dyes is calculated.

Fig. 4 is the histogram for the end-to-end distance of a 24-base

DNA ruler measured by NALMS fluorescence microscopy. Because the distance cannot have negative values and the mean distance is very close to the boundary value (i.e., zero), the distance distribution may exhibit a skew. As a result, a lognormal distribution may be a more appropriate description of the histogram than a Gaussian distribution (26). The lognormal fit to the histogram gives the end-to-end distance as $[8 - 2, 8 + 3]$ nm where 8 nm is the center of the lognormal fit. The 2- and 3-nm values are the width of the fitted lognormal function for the region to the left and to the right of the center value, respectively, and are a measure of the SE of the distance measurement. The expected end-to-end distance of a 24-base double-stranded B-form DNA ruler is 8 nm $[24 \text{ bases} \times (1 \text{ nm}/3 \text{ bases})]$. Therefore, the measured result agrees very well with the expected value.

Only traces showing two photobleaching events are used in this analysis; many spots showed only a single bleaching event, perhaps because one fluorophore had photobleached before observation. The nonzero baseline in the distance distribution can be attributed to a random spatial distribution of these single fluorophores, some pairs of which happen to lie within a measured spot.

The present experiments employ a CCD detector with effective pixel size of $a = 65.7$ nm and $S_{x,y} = 124.8$ nm. The events in Fig. 4 only include those dual-fluorophore traces with >500 accumulated counts at the peak pixel for the part of the trace used for centroid localization. The precision for centroid localization is better for the events with more counts collected, and thus the SE of the distance measurement in the histogram is mostly defined by the events close to the chosen threshold of collected counts. The threshold value corresponds to total counts $N = 11,300$ and the SD of the background is $b = 13$ counts. According to Eq. 3, this corresponds to $\sigma_{x0} = \sigma_{y0} = 1.8$ nm for each fluorophore. Thus, Eq. 4 gives the SE of the end-to-end distance measurement as $\langle \Delta d^2 \rangle^{1/2} = 2.5$ nm, which agrees well with the measured SE, i.e., the width of the lognormal fit of Fig. 4.

The above analysis assumes that the behavior of the fluorophores is time-invariant. If this assumption fails, it would be a source of error in position determination that must be assessed. As seen from Figs. 2 and 3, the fluorophore mean intensity is generally constant with statistical fluctuations. The variation in intensity of fluorophore 1 does not affect the localization result of its own centroid and only affects the fitted value of N_{00} . Any change in the emission intensity or position of fluorophore 1 between intervals 1 and 2 of the time trace would affect the calculated centroid location of fluorophore 2. A larger difference in the average emission behavior of fluorophore 1 would cause a larger error in the localization of fluorophore 2. This effect is illustrated in Fig. 5. Beginning with an individual distance measurement in the data for Fig. 4, in which each fluorophore had 500 counts for the peak pixel (measured distance in this instance was 5.9 ± 2.5 nm), the estimated intensity of fluorophore 1 was varied before subtraction from the data used to locate fluorophore 2. As seen from Fig. 5, the deviation of the distance estimate is within 1 nm for $<10\%$ variation in the intensity of fluorophore 1. For most events included in Fig. 4, the deviation of each image from its average behavior is $<12\%$, and usually the average behavior of fluorophore 1 is taken as the average of five or more images, and thus the average obtained this way has $<12\% \cdot (5)^{-1/2} = 5\%$ SE from the true average value. According to Fig. 5, this result corresponds to <0.3 -nm deviation in the centroid localization of fluorophore 2. This deviation is small compared with the other errors estimated from Eq. 4. Thus, Eq. 4 is a good estimation of the total error of the distance measurement in the experiment (see Fig. 4).

Fig. 6 shows the histogram for the end-to-end distance of a

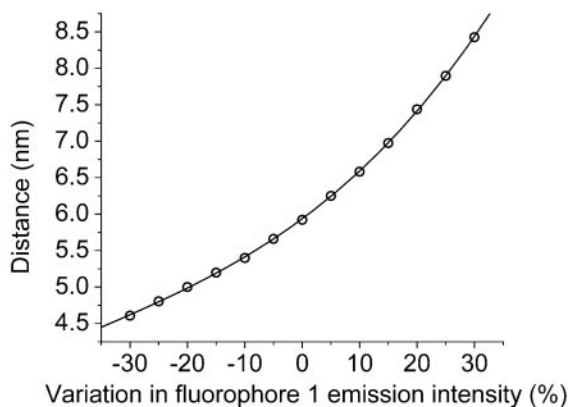


Fig. 5. Deviation of localized centroid value of fluorophore 2 due to variation in the intensity of fluorophore 1. The data were calculated as follows: taking N_{001} as the peak intensity of fluorophore 1 determined by centroid localization from the one-dye image, the data point at 5% variation was obtained by subtracting the contribution of fluorophore 1 with $N_{001} = 1.05 N_{001}$ from the two-dye image. Then, the centroid of fluorophore 2 was localized, and the distance between the two centroids was calculated. The data point at -5% variation was calculated by taking $N_{001} = 0.95 N_{001}$. All other data points were obtained in the same way. The dots are the data from the simulation and the curve is a power law fit to the data. The best cubic polynomial fit is $Y = 5.936 + 5.83 \times 10^{-2}X + 6.6 \times 10^{-4}X^2 + 5.8 \times 10^{-6}X^3$ nm.

40-base DNA ruler measured by NALMS microscopy. As in the case of the 24-base DNA ruler, the distance can only take nonnegative values. However, in this case, the mean distance is farther away from the boundary value than in the case of the 24-base DNA ruler and thus no obvious skew is observed in the distance distribution. A Gaussian function is used to fit the histogram, which gives an end-to-end distance of 13 ± 4 nm. This measurement agrees very well with the 13.3-nm [40 bases \times (1 nm/3 bases)] end-to-end distance expected for a 40-base B-form DNA ruler. Because the same threshold of counts is used as for the 24-base DNA ruler, Eq. 4 predicts a 2.5-nm SD in the distance measurement. The larger observed SD in this case probably reflects drift in the microscope focus over the relatively long time traces (up to 8 min) used in this analysis (compare <30-s traces for Fig. 4). The nonzero baseline in Fig. 6 is

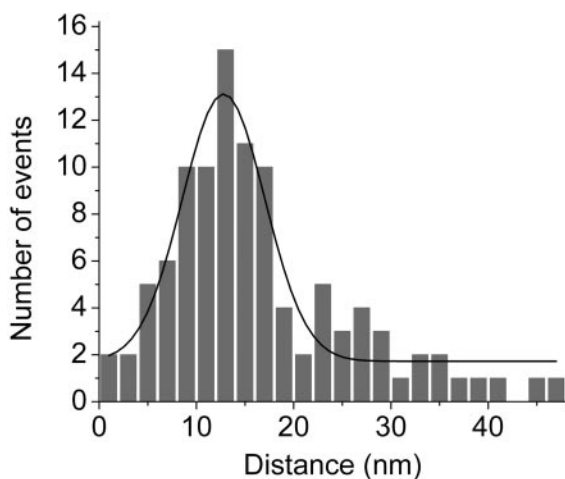


Fig. 6. Histogram of end-to-end distance measurements of a 40-base DNA ruler. The Gaussian fit gives the end-to-end distance as 13 ± 4 nm, where 13 nm is the location of the center of the Gaussian fit and 4 nm is the width of the fit.

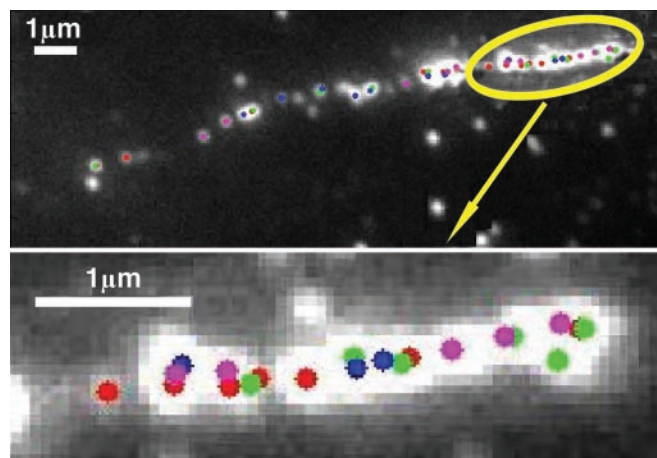


Fig. 7. DNA mapping with NALMS microscopy. The grayscale was chosen so that single molecules can be seen. The right part of the image is saturated because many bis-PNA molecules are bound to this region. A series of images was taken at rate of 1 frame per s until all of the fluorophores photobleached. Only the centroid localization results for fluorophores photobleached within the first four frames of images are shown, to avoid creating an overcrowded picture at the right part of the image (the overlabeled region). The colored dots show the centroids of the localized fluorophores. Fluorophores that photobleached in the same CCD image acquisition frame are shown with the same color; different colors are used for fluorophores that photobleached in different frames. The SD of the centroid localization varies between 7 and 2 nm, depending on the number of photons collected for each fluorophore.

attributed to the same cause as in the 24-base DNA ruler experiment.

The DNA ruler tests verify that NALMS fluorescence microscopy can resolve fluorophores that are 8 nm or more apart. We did not test whether even smaller distances can be resolved, although in principle the system should resolve fluorophores separated by more than the uncertainty in the distance measurement, which is determined by the uncertainty in centroid localization of fluorophores.

DNA Mapping with NALMS Microscopy. Fig. 7 shows a fluorescence image of λ -DNA bound by Alexa 488-labeled bis-PNA. Bis-PNA binds tightly to specific recognition sequences in double-stranded DNA (23). The pattern of these binding sites produces a physical map that would be specific for different DNA sequences. NALMS microscopy offers a method for resolving fluorescent probes bound to specific recognition sites in DNA. Under the long-exposure binding conditions used, the 7-base bis-PNA probes bind to more than just their specific recognition sites. Although this occurrence prevents reconstruction of an accurate map, the high number of bound dye molecules provides multiple single fluorophores that overlap in conventional microscopy, and thereby tests the resolving power of NALMS. In Fig. 7, every dye in the overlabeled region (i.e., rightmost part of the image) can be resolved and localized to within 10 nm (most within 7 nm and some within 2 nm), which is far beyond the capability of traditional optical microscopy or previous optical mapping studies. Thus, NALMS offers a resolution method for very-high-density physical mapping of individual DNA molecules.

Conclusion

Nanometer resolution of multiple single molecules can be achieved in fluorescence microscopy by combining centroid localization analysis and the inevitable photobleaching of single fluorophores. NALMS microscopy resolution is verified with nanoscale DNA rulers; single fluorescent molecules that

are 8 nm or more apart could be readily resolved with ≈ 2.5 -nm precision. The empirically determined limit of the resolution of NALMS microscopy is 8 nm or better, covering the gap between FRET-based (<10 nm) and diffraction-limited microscopy (>100 nm) measurements of the distance between two fluorophores.

In the present study, up to five spectrally identical fluorophores could be resolved; however, this is not necessarily the upper limit. In the experiment, we did not observe any influence of the 2-d spatial arrangement of the dye molecules on the resolution. However, for a diffraction-limited spot with more dye molecules, it will be harder to resolve every dye molecule in it, and the precision of the centroid localization for each dye molecule will in general deteriorate. The limit depends on the experimental conditions. The average total number of photons detected before photobleaching for dye molecules varies, depending on the dye molecules and buffer conditions, the N.A., and efficiency of the imaging system. The number of detected photons generally determines the precision of the centroid localization and the limit of the resolution. To reach the maximum resolving power, two conditions would help; lowering the laser illumination power, and using a faster CCD detector. Both conditions increase the probability to catch every photobleaching event. Of course, there are limiting factors, such as the background noise, the CCD noise, the quantum nature of the dye emission, and the sensitivity of the CCD. Also, active control of the drift in the microscope system will greatly help the measurement precision.

The requirement for application of NALMS microscopy is that individual photobleaching events are resolved and that the individual fluorophores are essentially stationary in time and

space. Thus, NALMS microscopy as performed here is limited to the measurement of static and dilutely labeled samples. Still, important questions can be addressed. NALMS microscopy will be a powerful approach for the creation of physical maps of DNA. It will be useful in obtaining high-resolution distributions of fluorescently labeled DNA-binding proteins. With the use of CCD detectors with on-chip gain and faster readout, NALMS microscopy will have application to study slow dynamics of molecular machines and even establish spatial distributions of fluorescently tagged macromolecules and assemblies *in vivo*.

Note. While this paper was under review, a paper appeared (27) reporting the use of photobleaching to resolve two fluorophores within the diffraction limit. Our work extends the concept to the nanometer-precision localization of multiple fluorophores that are unresolved in a static image. The image processing used in the present paper differs from that reported in ref. 27. These differences in numerical methods may affect the precision of fluorophore localization in certain circumstances and also the computation time for analyzing the images, particularly when multiple fluorophores are involved. As shown in this work, ultraresolution of multiple fluorophores will be important in many applications, including DNA mapping.

We thank Glenna Smith and Zheng Xie (Department of Chemistry, University of Chicago) for assistance with sample preparation for the DNA ruler test; Rebecca Stark and Katie Ryan (Department of Molecular Genetics and Cell Biology, University of Chicago) for assistance with sample preparation for demonstrating the application to DNA mapping; and Prof. Paul Selvin (Department of Physics, University of Illinois at Urbana-Champaign, Urbana) for stimulating discussions. This work was supported by David and Lucile Packard Foundation Grant 2001-17747, National Institutes of Health Grant GM067961, and a Seed Grant from the Institute for Biophysical Dynamics at the University of Chicago.

1. Born, M. & Wolf, E. (1997) *Principles of Optics* (Cambridge Univ. Press, Cambridge, U.K.).
2. Alberts, B., Bray, D., Lewis, J., Raff, M., Roberts, K. & Watson, J. D. (1994) *Molecular Biology of the Cell* (Garland, New York).
3. Clegg, R. M. (1996) in *Fluorescence Imaging Spectroscopy and Microscopy*, eds. Wang, X. F. & Henman, B. (Wiley, New York), pp. 179–251.
4. Lakowicz, J. R. (1999) *Principles of Fluorescence Spectroscopy* (Plenum, New York).
5. Gelles, J., Schnapp, B. J. & Sheetz, M. P. (1988) *Nature* **331**, 450–453.
6. Kubitscheck, U., Kückmann, O., Kues, T. & Peters, R. (2000) *Biophys. J.* **78**, 2170–2179.
7. Cheezum, M. K., Walker, W. F. & Guilford, W. H. (2001) *Biophys. J.* **81**, 2378–2388.
8. Yildiz, A., Forkey, J. N., McKinney, S. A., Ha, T., Goldman, Y. E. & Selvin, P. R. (2003) *Science* **300**, 2061–2065.
9. Yildiz, A., Tomishige, M., Vale, R. D. & Selvin, P. R. (2004) *Science* **303**, 676–678.
10. Lacoste, T. D., Michalet, X., Pinaud, F., Chemla, D. S., Alivisatos, A. P. & Weiss, S. (2000) *Proc. Natl. Acad. Sci. USA* **97**, 9461–9466.
11. Hell, S. & Stelzer, E. H. K. (1992) *J. Opt. Soc. Am. A* **9**, 2159–2166.
12. Xie, X. S. & Dunn, R. C. (1994) *Science* **265**, 361–364.
13. Rothenfluh, H. S., Gibbs, A. J., Blanden, R. V. & Steele, E. J. (1994) *Proc. Natl. Acad. Sci. USA* **91**, 12163–12167.
14. Dineen, S. S., Bradshaw, M. & Johnson, E. A. (2003) *Curr. Microbiol.* **46**, 345–352.
15. Balakirev, E. S., Balakirev, E. I. & Ayala, F. J. (2002) *Gene* **288**, 167–177.
16. França, L. T. C., Carrilho, E. & Kist, T. B. L. (2002) *Q. Rev. Biophys.* **35**, 169–200.
17. Braslavsky, I., Hebert, B., Kartalov, E. & Quake, S. R. (2003) *Proc. Natl. Acad. Sci. USA* **100**, 3960–3964.
18. Jing, J., Reed, J., Huang, J., Hu, X., Clarke, V., Edington, J., Housman, D., Anantharaman, T. S., Huff, E. J., Mishra, B., *et al.* (1998) *Proc. Natl. Acad. Sci. USA* **95**, 8046–8051.
19. Nelson, P. (2003) *Biological Physics* (Freeman, New York).
20. Ha, T. (2001) *Methods* **25**, 78–86.
21. Zheng, X., Srividya, N., Sosnick, T. R., Pan, T. & Scherer, N. F. (2004) *Proc. Natl. Acad. Sci. USA* **101**, 534–539.
22. Michalet, X., Ekong, R., Fougereuse, F., Rousseaux, S., Schurra, C., Hornigold, N., van Slegtenhorst, M., Wolfe, J., Povey, S., Beckmann, J. S. & Bensimon, A. (1997) *Science* **277**, 1518–1523.
23. Kuhn, H., Demidov, V. V., Frank-Kamenetskii, M. D. & Nielsen, P. E. (1998) *Nucleic Acids Res.* **26**, 582–587.
24. Thompson, R. E., Larson, D. R. & Webb, W. W. (2002) *Biophys. J.* **82**, 2775–2783.
25. Ha, T., Enderle, T., Chemla, D. S., Selvin, P. R. & Weiss, S. (1997) *Chem. Phys. Lett.* **271**, 1–5.
26. Limpert, E., Stahel, W. A. & Abbt, M. (2001) *Bioscience* **51**, 341–352.
27. Gordon, M. P., Ha, T. & Selvin, P. R. (2004) *Proc. Natl. Acad. Sci. USA* **101**, 6462–6465.